Available online at www.sciencedirect.com
SCIENCE DIRECT®
Sensors and Actuators A 119 (2005) 489–501
SENSORS AND ACTUATORS A PHYSICAL
www.elsevier.com/locate/sna

Magnetically bistable actuator Part 1. Ultra-low switching energy and modeling

Gary D. Gray Jr., Paul A. Kohl*

School of Chemical Engineering, Georgia Institute of Technology, Atlanta, GA 30332-0100, USA

Received 26 July 2004; received in revised form 19 October 2004; accepted 21 October 2004
Available online 8 December 2004

Abstract

The optimal design space for a bistable magnetic actuator with ultra-low actuation energy and large actuation distance (100 μm) has been modeled. Attention was paid to minimizing the energy expended to minimize heat dissipation and power consumption so that the device could be used over a wide temperature range, including cryogenic environments. A more desirable switching regime existing for low magnetic fields (10 mT) was found that requires shorter pulses (microsecond versus millisecond) and lower actuation energy (<5 μJ versus 100 μJ) than designs outside of this space. The device was modeled to latch in two states, based on the interaction of the magnetic actuator with an external magnetic field.

Keywords: Magnetic MEMS; Actuators; Microrelays; Modeling

1. Introduction

Microelectromechanical system (MEMS) technology enables the batch fabrication of micro-miniature mechanical structures, devices, and systems having length scales normally less than 1 mm. Additionally, MEMS technology exhibits many of the advantages indigenous to integrated circuit (IC) technologies such as cost control through batch fabrication, device-to-device consistency from lithography and etching techniques, and performance advancements from dimensional downscaling. This leads to a significant cost, size and weight reduction compared to existing devices [2].

Many MEMS designs use electrostatic, thermal, or magnetostatic actuation to move the micro-fabricated parts. Electrostatically activated cantilever beams have been used as discrete relays, as well as tunable capacitors [3–5]. They have the advantage over most early magnetically actuated devices in that they require little current, and low continuous power in supplying a constant voltage to hold the desired state of the switch. However, the effects of static actuation fall off as the gap distance squared and consequently large gap distances are difficult to achieve. Further, the applied actuation voltage can be significant. Magnetically actuated MEMS are able to function over larger gap distances since increasing the magnetic volume can increase the magnetic torque. There are two common actuation mechanisms used by a majority of magnetic MEMS devices. The first approach is to create a magnetic torque acting on a magnetic element that aligns the magnetic material with some applied external field. Judy and Muller developed magnetically actuated cantilevers that were individually addressable by in-plane coils [6]. The shape of the ferromagnet had a significant influence over the magnetization direction, confining the magnetization vector to the plane of the ferromagnet. The in-plane coil produces a magnetic field, and the cantilever beam moves toward the external field, minimizing the energy of the system. In addition, Judy and Muller developed a comprehensive static actuation model [6]. Ahn and Allen developed an early magnetic actuator with a multilevel meander magnetic core [7], and Taylor and Allen later improved the design to achieve <50 mΩ contact resistance with >100 μN contact force [8]; however, the "dead

* Corresponding author. Tel.: +1 4048942893; fax: +1 4048942866.
E-mail address: paul.kohl@chbe.gatech.edu (P.A. Kohl).

0924-4247/$ – see front matter © 2004 Elsevier B.V. All rights reserved.
doi:10.1016/j.sna.2004.10.027

legs" and small actuation distances limit its use for many applications, including high-performance RF switch applications. The second approach makes use of a low reluctance path through the entire device that creates a force to hold the device in a given state. Wright et al. [9] developed a high force actuator using this method. Also, Companu et al. [10] developed a bistable microvalve that latches in order to close one of two low reluctance paths, using a patterned coil to switch the device. However, these methods have not suitably addressed the issue of reducing power consumption, which is increasingly critical for use in cryogenic environments, and the designs do not lend themselves to large actuation distances. Additionally, the very nature of a low reluctance core requires a large volume of ferromagnetic material be placed in the electrical path, potentially degrading electrical performance and increasing thermal stresses at elevated or cryogenic temperatures.

Ruan et al. have successfully developed and demonstrated a mechanism for magnetic latching that requires an external magnetic field and a patterned in-plane coil to control the dynamics of a magnetic cantilever [1]. Bistable behavior is achieved using a permanent magnet to provide the latch, without the need for a low reluctance path. The clear benefit of this approach is that since it is the permanent magnet that provides the latching force, power is only required while changing the latched state of the device. In Ruan's design, a magnetic torque is exerted on a beam having a soft magnetic material (permalloy) electroplated on a gold seed layer and is held latched by an external magnetic field [1]. The device is switched by momentarily activating a magnetic field drive coil patterned in the plane of the substrate. The torque created by the interaction of the permalloy on the cantilever and the field generated by the external magnet causes latching in one of two possible configurations: upstate and downstate, as shown in Fig. 1. The beam is anchored at one end, and the permalloy is patterned in such a way that its length is the dominant geometrical dimension. This causes the beam to occupy one of two magnetic states under the influence of an external magnetic field. The two preferred magnetization directions are antiparallel, both lying along the beam's length. The magnetic torque is represented by $V\vec{M} \times \vec{B}$, where $\vec{M}$ is the magnetization vector of the beam, V the volume of the magnetic material deposited on the beam, and $\vec{B}$ is the external magnetic field. Thus, the magnetic torque tends to move the beam such that it is more aligned with the external field. In Fig. 1(a), B_{external} would move the beam to a more vertical position. The beam remains magnetized by the magnetic field provided from the permanent magnetic source attached to the substrate [1].

In order to move the device from the upstate to the downstate, it is necessary to reverse the direction of the magnetization vector along the permalloy. To accomplish this, the local magnetic field in the vicinity of the beam must have a positive component directed towards the opposite side of the beam in Fig. 1. Since the local magnetic field supplied by the permanent magnet cannot be changed, an alternative

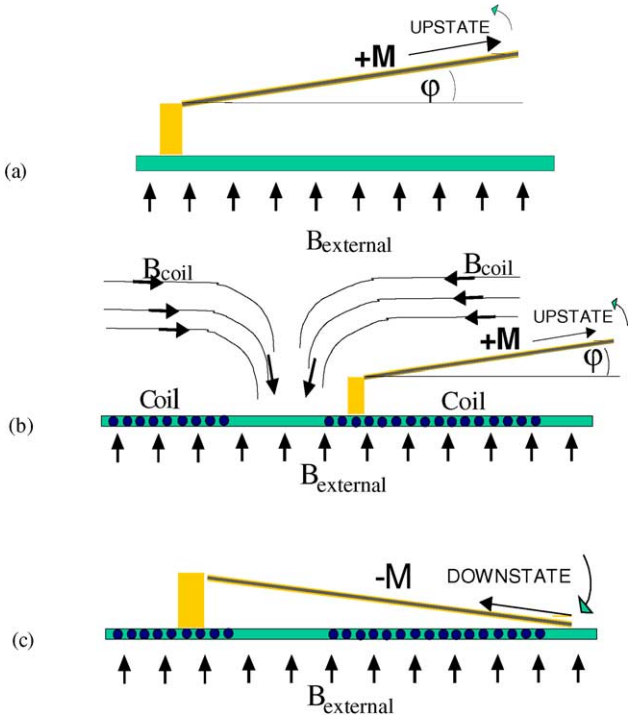

Fig. 1. (a) Magnetic beam device with two stable states. (b) Switching mechanism between states. (c) New equilibrium position.

magnetic source must be used. One method to overcome the component of the external magnetic field holding the beam in the upstate (i.e., $B_{\text{external}} \sin\varphi$, where φ is the angle the beam makes with the horizontal) is to create a second magnetic field opposing B_{external}, such as through the use of a current carrying coil. If the coil were placed as shown in Fig. 1(b), the coil's magnetic field would have a large horizontal component in the vicinity of the beam. In order for the direction of the magnetization to flip, the following inequality must hold (assuming B_{coil} is orthogonal to B_{external}):

$$B_{\text{coil}} \cos\varphi > B_{\text{external}} \sin\gamma + H_{\text{c}} - \frac{\sqrt{N_{\text{l}}^2 + \theta^2}}{VB_{\text{external}}} \Gamma_{\text{elastic}} \quad (1)$$

Here, γ is the angle between the magnetization direction and the direction of the permanent external magnetic field, H_{c} the coercivity of the permalloy, N_{l} the demagnetization factor of the beam along the length, θ the angle the magnetization vector is pulled away from the plane of the ferromagnetic material due to the anisotropy torque, and Γ_{elastic} the elastic torque acting on the beam in the current position. Eq. (1) establishes a lower bound on the externally applied B_{coil} field, which in turn establishes the minimum current that is needed for switching the device as a function of the device position (φ) and external field strength B_{external}. This inequality will be developed in the body of this paper and will be shown to have a higher value compared to the $B_{\text{coil}} > B_{\text{external}} \sin\varphi$ criterion used previously [1]. When the inequality in Eq. (1) is satisfied, the net magnetization switches to the opposite

side, and the magnetic torque changes to counterclockwise in Fig. 1. The beam then begins a downward movement and eventually occupies the downstate (Fig. 1(c)). Power must be supplied to the coil for a time such that when the coil is terminated the beam will not magnetize in the original direction. For the 30 kA/m magnetic fields reported in Ruan's work, this requires the coil remain powered during a significant fraction of the total time (∼50%) for the beam to travel the actuation distance [1]. Once the current through the coil is terminated, the external magnetic field provided by the permanent magnet holds the device in the downward state. When the beam is in the downstate, the counterclockwise motion tends to partially align the beam magnetization vector with the external magnetic field [1].

The goal of this work is to apply the concepts of magnetic bistability to the design of a large-throw, energy-efficient MEMS actuator. This paper presents improvements in the design and analysis for a more energy-efficient device. Specifically, this is done through: (1) minimization of the power consumption by identifying a regime where shorter switching pulses can be used, and (2) analysis of the design space for such devices.

2. Design criterion

2.1. Mechanical design

In previous work, the static out-of-plane bending of electrostatic cantilever beams was determined by the thickness of a hard gold, stressed layer electroplated onto the beam surface [4,5]. Then, when the beam was to be displaced by force, the entire structure and hinges would bend, yielding to the electrostatic attraction. Partial hinges (narrow segments of metal connecting the cantilever to the anchor) would bend more easily. The required force was reduced by a factor equal to the relative width of the hinge to the width of the beam. If the beam shape from the previous work were to be used in the fabrication of the magnetically actuated devices, a uniform thickness of permalloy on the beam and hinges would render the device exceedingly stiff. For example, suppose that such a beam/hinge device needed to be deflected a distance x for a given RF isolation to be achieved. Next suppose that the permalloy thickness, t_0, present on the gold beam/hinge (total thickness T) surface results in a deflection x_0. Assuming that x_0 is less than x, the application of Δt_0 more permalloy would result in a new magnetic moment, M_{new}, given by Eq. (2), where M_{old} is the magnetic moment from permalloy thickness t_0.

$$\frac{M_{\text{new}}}{M_{\text{old}}} = \frac{t_0 + \Delta t_0}{t_0} = 1 + \frac{\Delta t_0}{t_0} \tag{2}$$

This is due to the fact that the volume of permalloy is linearly related to the magnetic moment at saturation. However, the new moment of inertia, I_{new}, of the beam has now increased by the factor shown in Eq. (3), as compared to the old moment of inertia, I_{old}.

$$\frac{I_{\text{new}}}{I_{\text{old}}} = \left(\frac{T + t_0 + \Delta t_0}{T + t_0}\right)^3 = \left(1 + \frac{\Delta t_0}{t_0 + T}\right)^3 \tag{3}$$

The ratio $M/(IE)$ gives the inverse of the radius of curvature of the beam, where E is the elastic modulus of the beam material [11]. In this manner, the ratio of the new curvature, r_{new}, to the old curvature, r_{old}, may be written as:

$$\frac{r_{\text{old}}}{r_{\text{new}}} = \frac{1 + (\Delta t_0/t_0)}{(1 + (\Delta t_0/(t_0 + T)))^3} \tag{4}$$

When the value of the RHS of Eq. (4) is greater than 1, the ratio of the magnetic moment to the moment of inertia increases with the application of additional permalloy. This translates into a net increase in the deflection of the beam. However, there exists a maximum deflection possible for a device of a given geometry in a uniform magnetic field. This critical condition is found when the RHS of Eq. (4) is set equal to unity. Neglecting higher order terms in Δt_0, it is found that the criterion for further beam deflection by application of more permalloy is $t_0 \leq T/2$. Thus, the beam will only deflect further under the addition of more permalloy if the previous permalloy thickness were less than half the non-permalloy beam thickness. While this geometry may result in significant deflections for very thin beam designs (<1 μm), hinges of this thickness are very fragile and difficult to use. Since there may only be a lower bound on T, it would be nonsensical to utilize a design that would penalize the resultant deflection by generating larger magnetic moments.

This necessitates a beam design with reduced stiffness in some areas, allowing a greater degree of bending in the hinge region while maintaining adequate rigidity along the actuator itself. This could be achieved by the use of thinner hinges near the beam anchor. Instead of plating permalloy on the entire device, permalloy can be selectively deposited on a portion of the beam. With this type of design, the stiffness of the hinge region does not depend on the amount of permalloy present, and Eq. (4) reduces to:

$$r_{\text{new}} = \frac{r_{\text{old}}}{1 + (\Delta t_0/t_0)} \tag{5}$$

This results in a lower radius of curvature (and therefore greater beam deflection) with further application of permalloy thickness. This holds true under the assumptions that the hinge bending remains elastic and the permalloy is magnetically saturated. The permalloy-plated areas may be considered as a rigid plate, and the deflection of the beam predominantly results from bending the non-permalloy areas. The magnetic material may be clad in gold to cancel out any mechanical bending that would otherwise occur upon cooling due to the thermal mismatches between the gold and the permalloy.

2.2. Magnetic element design

An expression for the magnetization for soft magnetic materials has been previously given by Judy and Muller [6].

$$M = \min\left\{\frac{B\sin\gamma \pm H_c}{\sqrt{N_l^2\cos^2\theta + N_t^2\sin^2\theta}}, M_{sat}\right\},$$
$$\gamma = \phi + \theta - \alpha \quad (6)$$

where B is the external magnetic field, α the angle the external field makes with the vertical, H_c the coercivity of the ferromagnetic material, N_l and N_t the demagnetization factors due to the shape of the ferromagnetic element along the length and thickness, respectively, M_{sat} the saturation value of the ferromagnetic material, and θ an angle the magnetization vector is pulled away from the plane of the ferromagnet. The magnetic torque for small deflection angles (valid because of the angular limits imposed by the two substrates) is given by

$$\Gamma_{magnetic} = \operatorname{sgn}\gamma \min\left\{\frac{B\sin|\gamma| \pm H_c}{\sqrt{N_l{}^2 + \theta^2}}, M_{sat}\right\} VB\cos\gamma \quad (7)$$

where sgn(γ) returns the sign of the argument, allowing for positive and negative values of M, depending on the direction of magnetization, sin(θ) has been replaced by θ, and N_t has been approximated by unity for the high aspect ratio (length/thickness) Ni/Fe shapes of interest. The sign of the coercivity is positive if the ferromagnetic material was last magnetized in the upper latched state and negative if last magnetized in the lower latched state. A balance on the magnetization vector, M, requires that the magnetic torque that acts to bend M out-of-plane of the permalloy is balanced by the anisotropy torque which acts to pull M back in-plane. For polycrystalline Ni/Fe alloys under normal stress, the only major form of anisotropy in the ferromagnetic material is due to shape anisotropy [6], then the anisotropy torque is given by Eq. (8). In the case of saturation, the angle which the magnetization vector is rotated out-of-plane, θ, is the solution to

$$\Gamma_{magnetic} = \Gamma_{anisotropy},$$
$$\Gamma_{anisotropy} = \frac{N_t - N_l}{2} VM_{sat}^2 \sin(2\theta) \quad (8)$$

By equating the magnetic torque to the anisotropy torque, Eq. (8), it can be shown that for saturated specimens the magnitude of θ is bounded by 0.01 rad for external magnetic fields in the 10 mT range. Therefore, θ may indeed become significant relative to N_l and have a large influence on the value of the magnetization (Eq. (6)) due to the impact on the denominator.

It should be noted that $\Gamma_{magnetic}$ scales quadratically with the external field at values of φ less than that at which the magnetic material becomes saturated. For values of φ greater than this, $\Gamma_{magnetic}$ scales linearly with the external field. At equilibrium, the magnetic torque will exceed the anisotropy torque; however, if a contact force is present between the contact pad and the beam tip, then the magnetic and anisotropic torques will not equal the elastic bending torque of the hinges.

For a given design and value of φ, the above system can be solved for θ and the torques. Judy and Muller [6] showed the importance of accurate determination of both the coercivity and the demagnetization of the ferromagnetic material in modeling magnetic actuator responses at low applied magnetic field levels; however, we contend that accurate determination of the angle θ is also critical in predicting the sensitivity of the degree of magnetization with rising magnetic field.

It can be seen from Eq. (6) that the rate of approach to saturation of the ferromagnetic material is strongly influenced by both the demagnetization value and the angle the magnetization vector makes with the plane of the magnetic material, θ. Increased levels of magnetization at a given field level are desirable since this results in a greater magnetic torque, potentially increasing the potential angular range of motion of the beam and improving the contact force between the beam and the substrate. Therefore, patterning the magnetic actuators to provide a greater anisotropy could greatly enhance the magnetization characteristics. However, in the limit of high anisotropy, the influence of θ becomes more significant, and further reduction of N_l no longer results in the reduction of the external field needed to produce a given magnetization. Since θ is tied to the magnetic torque through Eq. (8), decreasing θ is now most readily accomplished by reduction in the background external magnetic field.

2.3. Coil design

A conductor carrying a current, I, produces a magnetic field, H, as given by the Biot and Savart law [12]. For a square planar coil, the calculated magnetic field produced is given by

$$H_{total} = \sum_{i=1}^{N}\sum_{j=1}^{4} |H_{i,j}|(\vec{z}\cos\varepsilon_{i,j} + \vec{r}\sin\varepsilon_{i,j}) \quad (9)$$

where $H_{i,j}$ is the field due the jth side of the ith turn of the coil, ε the angle the line connecting the field point to the nearest point of segment i, j makes with the line side connecting the coil center to coil side i, j, $\vec{r}$ the unit vector in the radial direction, and $\vec{z}$ the unit vector orthogonal to the plane of the coil. The contributions due to each of the current segments $H_{i,j}$ may be calculated by the following:

$$|H_{i,j}| = \frac{I}{2\pi r_{i,j}}\left[\frac{L_{i,j}}{(L_{i,j}{}^2 + r_{i,j}{}^2)^{1/2}}\right] \quad (10)$$

Here, L is half the length of the segment i, j, I the current supplied through the coil, and r_{ij} the distance on the midline from segment i, j to the field point. This analysis holds provided the field point lies in the midplane of one of the coil side. This is acceptable as placement of the magnetic material of the MEMS device orthogonal to the coil side and at the midpoint of one of the coil sides results in only compo-

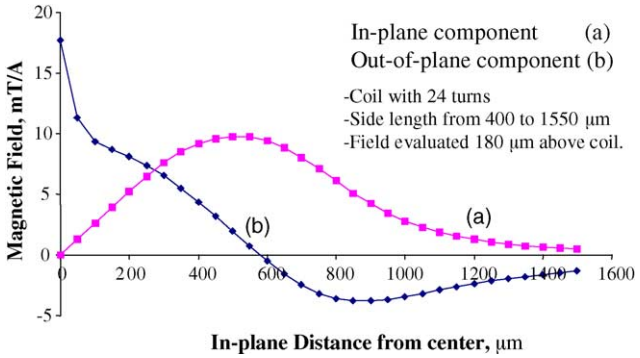

Fig. 2. In-plane and out-of-plane components of field generated from a 24-turn rectangular coil.

nents along the beam length to be developed in the plane of the magnetic material. The designs were evaluated based on the relative magnitude of the in-plane and out-of-plane field components at a distance equal to the placement of the coil relative to the ferromagnetic material.

Both circular and square coils were evaluated. Each coil type was evaluated with 24 turns with an average spacing of 50 μm. The coil with circular turns yields a broader range of high radial magnetic field, but also generates a significant out-of-plane field component that, along with low external field levels, provides a significant degree of disturbance, and thus affects the background field levels. Fig. 2 shows the field produced by the rectangular coil, as calculated from Eq. (9). The square coil has a higher maximum field generation, but is over a narrower range. Also, the out-of-plane component is significantly less than the out-of-plane component for the circular design, and experiences a sign change midway along the range of large radial field levels, as shown in Fig. 2. This results in an averaging effect of the out-of-plane component over a certain range, meaning that proper design could eliminate consideration of this component as a perturbation to the background external magnetic field. For these reasons the square coil design was chosen. The radial component, used in performing the switching, falls off rapidly with increasing r. At the edge of the coil, 1550 μm, the radial component is only 10% of its maximum value. A 700 μm magnetic beam would see an average field of 50% of the maximum radial field if properly placed. This is still five times greater than the field that would be generated just off the coil edge. This means that devices could be placed as close together as adjacent coils with no concern of switching interference between neighboring devices. In addition, coil size could be significantly reduced without concern for coil-to-coil interference. Multilevel coils have been utilized by others [13], and could be considered here for added field strength and increased spatial density.

2.4. Establishing the design space

A schematic diagram showing the interplay of the various geometrical and magnetic parameters is presented in Fig. 3. Both the magnetic torque due to the magnetic field acting on the ferromagnetic volume of the cantilever and the elastic torque required to flex the hinges are graphed as a function of the angle, φ, that the beam tip makes with the horizontal. Regions corresponding to latching behavior are detailed with Roman numerals. The model includes the initial angular displacement of the cantilever, as well as the angle the external magnetic field makes with the vertical. Fig. 3 also shows the angular placements of the upper and lower substrates. Such a graphical representation provides for a more complete understanding of the working device. The bending torque is a linear function of this angle (provided the hinge strain re-

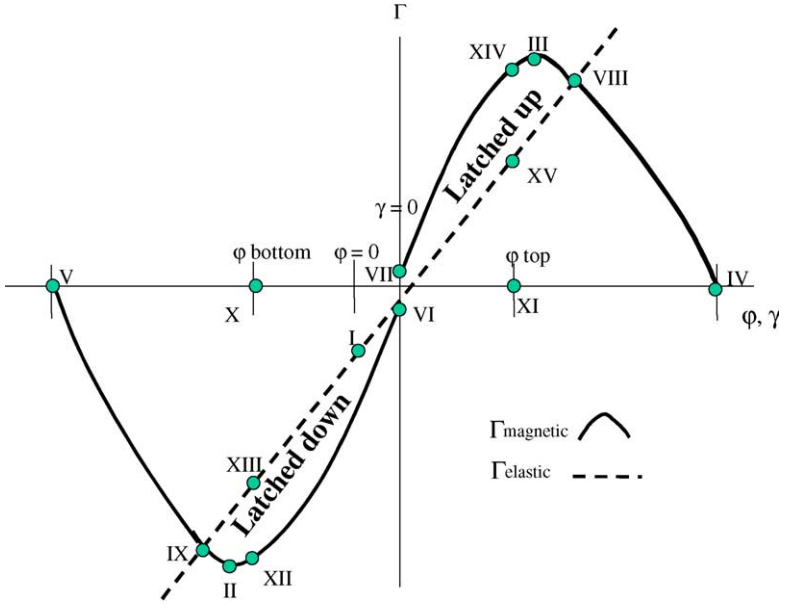

Fig. 3. Design space for high isolation bistable magnetic actuator.

mains in the elastic regime) as shown by the dashed line in Fig. 3. The slope of the elastic torque is equal to the stiffness, k_φ, of the hinge configuration. The intercept is nonzero if the beam has an initial deflection. Eq. (11) gives the form of the elastic torque.

$$\Gamma_{\text{elastic}} = k_\phi(\phi - \phi^0) \tag{11}$$

For an initial deflection of the beam, φ^0, the intercept of the elastic torque versus φ line will be $-k_\varphi\varphi^0$ (point I). The angular stiffness of the hinge configuration depends on its geometry through the third power of the hinge thickness, the first power of beam width, and inversely with the length.

Incorporation of a nonzero initial deflection angle gives the model an additional level of robustness, since this allows stresses developed in the hinges due to sputtering and/or electroplating of gold to be considered, as well as any other fabrication inconsistencies which can affect the hinge curvature. The initial deflection removes the system symmetry, causing a greater difference between Γ_{magnetic} and Γ_{elastic} in one state versus the other. This initial deflection tends to decrease the stability of one latched state in favor of increasing the stability of the other state. This effect can be mitigated by control of the angle of the permanent external magnetic field, α. Decreasing the angle between the initial state of the beam and the external magnetic field reduces the stability of the upper latched state, while restoring stability to the lower latched state.

The magnetic torque (Fig. 3, solid line) is a function of the geometry of the ferromagnetic material and the external magnetic field. Eq. (7) gave the form of the magnetic torque. The form of Eq. (7) generates two branches for Γ_{magnetic}, one for $\gamma > 0$ corresponding to a potential upper-latched state, and one for $\gamma < 0$ corresponding to a potential lower-latched state. Each branch increases with an increase in the magnitude of φ, and reaches a maximum at which point the ferromagnetic material is saturated, $M = M_{\text{sat}}$ (points II and III of Fig. 3), and then decreases as $\cos(\gamma)$. The magnetic torque is gradually reduced to zero at angles of φ such that $\gamma = \pm\pi/2$ (points IV and V). The value of Γ_{magnetic} when γ equals zero is determined by Eq. (7) and depends on the previously magnetized state of the ferromagnetic material. The intercept values are given by

$$\Gamma_{\text{magnetic}}(\gamma = 0) = \pm VB \min\left(1, \frac{H_c}{\sqrt{N_l{}^2 + \theta^2}}\right) \tag{12}$$

The positive sign should be used for a beam most recently magnetized to yield a positive φ. The intercept value for the $\gamma < 0$ branch will be negative (point VI), and the intercept value for the $\gamma > 0$ (point VII) branch will be positive. The value of θ in Eq. (12) can be calculated by equating the elastic torque and the anisotropy torque. The distance between the two intercepts is obtained by subtraction, and is shown in

$$\Delta\Gamma_{\text{magnetic}}(\gamma = 0) = 2VB \min\left(1, \frac{H_c}{\sqrt{N_l{}^2 + \theta^2}}\right) \tag{13}$$

This value gives a measure of the separation between the two branches of the magnetic torque in the region of small γ. Eq. (13) decreases with increasing softness (lower H_c) of the magnetic material, shape anisotropy, and external field. Larger $\Delta\Gamma$ corresponds to a higher degree of minimum magnetization and larger contact forces, but also may result in larger switching energy.

In order for a stable solution to exist and latching to occur, there must exist a value of φ such that the following expression holds:

$$|\Gamma_{\text{magnetic}}| > |\Gamma_{\text{elastic}}| \tag{14}$$

Thus, the magnetic torque generated must exceed the elastic torque resisting the angular movement. In Fig. 3, these stable regions where the magnitude of the magnetic torque exceeds the magnitude of the elastic torque, are shown and labeled as “latched up” and “latched down”. If unimpeded, such as by the presence of a substrate, the actuator will move to an equilibrium position where the magnetic torque and elastic torque are balanced when magnetized. These positions are given as points VIII and IX. These points correspond to the widest span of φ that can be obtained with a given device design and magnetic field. In order for the beam to make contact with either the top or bottom substrates the values φ_{top} and φ_{bottom} must satisfy the following condition.

$$|\varphi_{\text{top}}| < |\varphi_{\max}|, \quad \text{or} \quad |\varphi_{\text{bottom}}| < |\varphi_{\min}| \tag{15}$$

This is equivalent to stating that the range of φ over which stable solutions exist must bound the values of φ corresponding to the latched up and latched down states. At such values of φ_{top} (XI) and φ_{bottom} (X), the magnetic torque exceeds the elastic torque. Graphically, this excess is the distance between points XII and XIII for the latched up state and points XIV and XV for the latched down state. The magnitude of this excess is related to the contact force between the top/bottom contact and the tip of the cantilever. Therefore, it is also some measure of the quality of contact between the two surfaces.

2.5. Optimized designs

Once a design is in hand that exhibits stable latched up and latched down states, the following parameters determine the attractiveness of the design: large gap distance, low cost, good contact force, and moderate magnetic field levels. In the case of an RF switch for example, the electrical isolation between transmission lines is a strong function of the geometrical arrangement of the transmission lines, improved by increase in their separation. Therefore, this is a case where large gap distances are desirable. However, once φ_{top} and φ_{bottom} begin to approach the values $\varphi_{\max}$ and $\varphi_{\min}$, higher isolation comes at the cost of reduced contact force. Furthermore, once φ_{top} and φ_{bottom} surpass given values of $\varphi_{\max}$ and $\varphi_{\min}$, changes must be made that either reduce the slope of Γ_{elastic} (reduction in hinge stiffness) or increase in Γ_{magnetic} (through further anisotropy, increased magnetic field). Re-

duction in hinge stiffness is achieved by reducing the hinge thickness. Increased contact force provides for a more stable latched position, and lower contact resistance [12], which is significant for potential electrical applications. Higher contact force can be achieved by increasing the magnetic field required to switch the device from one latched position to another, however at the expense of large coil currents (and switching energy).

2.6. Contact force modeling

For the beam to have a low resistance electrical contact, it is necessary to analyze the moments acting on the actuator,

$$\Gamma_{\text{magnetic}} - \Gamma_{\text{elastic}} - \Gamma_{\text{contact}} = 0 \tag{16}$$

where Γ_{contact} is the torque due to the contact force. The magnetic and elastic torques have been given previously (Eqs. (7) and (11)). The torque due to the point of contact is given by

$$\Gamma_{\text{contact}} = F_{\text{contact}} X \cos\phi \tag{17}$$

where X is the length of the permalloy section of the beam. Substitution of the above equations yields an expression for F_{contact} in terms of the previously defined variables as follows:

$$F_{\text{contact}} = \frac{VB \min\{(B \sin|\gamma| + \text{sgn}(\gamma)H_c)/\sqrt{N_l{}^2 + \theta^2},\, M_{\text{sat}}\}\text{sgn}(\gamma)\cos\gamma - k_\phi(\phi - \phi^0)}{X\cos(\phi)} \tag{18}$$

Here it can be seen that for a given design, the contact force at a given position is proportional to the difference between the magnetic and elastic torques evaluated at that position. Furthermore, both the volume of the magnetic element and the angular hinge stiffness scale as s^3, while the denominator scales as s (where s is the scaling factor of the system size). Therefore the contact force decreases as the system scale is decreased. For a permalloy volume 1000 μm × 100 μm × 10 μm in a 10 mT external magnetic field and a permalloy length, X, of 1000 μm, the maximal contact force is 8 μN, assuming complete saturation and negligible elastic torque. Hosaka [14] has shown that contact forces greater than 50 μN are necessary to achieve contact resistances below 100 mΩ, but smaller forces in the tens of μN may yield contact resistances in the 200 mΩ range. Therefore a volume greater than 10^6 μm^3 may be required.

3. Results

To investigate the switching energies needed to actuate this type of magnetically actuated device, three candidate designs were chosen which would serve to illustrate the variations in switching speed and switching energy. These variations are summarized in Table 1. Each design was generated to yield two stable equilibria, with contact forces ranging from 5 to 20 μN in a magnetic field of 10 mT. Each of the three designs was given a different degree of shape anisotropy, ranging from a single permalloy slab ($N_l = 0.014$) to long, narrow strips ($N_l = 0.0013$). This was done so that the effect of anisotropy on switching characteristics, in particularly those used in justifying a low-energy switching regime, could be investigated. Additionally, shape anisotropy was varied in order to generate greater magnetic element movement at low magnetic fields. The beam length was varied in order to investigate switching speed on device size, as well as to quantify the additional power requirement anticipated for smaller devices. In its simplest form Eq. (1) requires that the magnetic field produced by the integrated coil be of the same size as the component of the external field in-plane with the cantilever beam. Smaller devices require a greater angular distance between the upstate and downstate, requiring the coil overcomes a larger component of the external magnetic field. Required values of the upper and lower substrate angles to achieve 100 μm actuation distance, φ_{top} and φ_{bottom}, are shown in Table 1 for each device. The hinge thickness was 2 μm for each design.

Graphical analysis of designs 1–3 were performed and are shown in Figs. 4–6, respectively. Designs 1 and 3 are shown with an external field of 10 mT and design 2 with 25 mT, since the lower magnetization values in this design required a minimum magnetic field strength for latching greater than 10 mT. For each latched state the magnetic torque line must exceed the elastic torque (curve a). The upper latched position for each device (point I) is located at the intersection of the upper magnetic torque line (curve b) with the $\varphi = \varphi_{\text{up}}$ line. Similarly, the lower latched position for each device (point II) is located at the intersection of the lower magnetic torque line (curve c) with the $\varphi = \varphi_{\text{down}}$ line. The vertical lines mark the angular range of motion of the device, allowed by the pres-

Table 1
Geometries of three candidate devices

Design	Ni/Fe design	Shape demagnetization factor	Hinge design	Angular range for 100 μm separation
1	Eight strips; each 940 μm long, 30 μm wide, and 12 μm thick. Volume = 2.7×10^6 μm^3	$N_l = 1.3 \times 10^{-3}$; $N_t = 0.95$	Two hinges; 260 μm long, 40 μm wide, 2 μm thick	φ_{down}: −0.027 rad; φ_{up}: 0.063 rad
2	One section; 500 μm long, 200 μm wide, and 12 μm thick. Volume = 1.2×10^6 μm^3	$N_l = 1.4 \times 10^{-2}$; $N_t = 0.95$	Two hinges; 270 μm long, 50 μm wide, 2 μm thick	φ_{down}: −0.050 rad; φ_{up}: 0.112 rad
3	Four strips; each 800 μm long, 30 μm wide, and 12 μm thick. Volume = 8.6×10^5 μm^3	$N_l = 1.3 \times 10^{-3}$; $N_t = 0.95$	Two hinges; 290 μm long, 30 μm wide, 2 μm thick	φ_{down}: −0.027 rad; φ_{up}: 0.063 rad

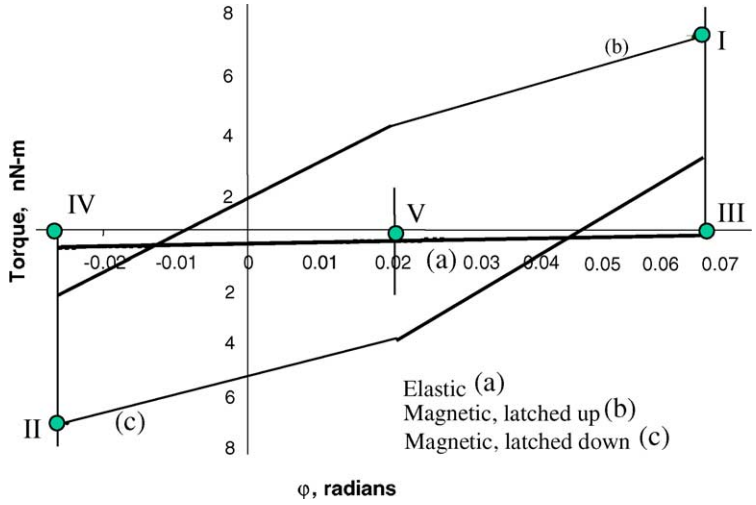

Fig. 4. Stability schematic for a type-1 magnetic actuator in a 10 mT external magnetic field. The initial upward angular deflection is approximately 0.1 rad.

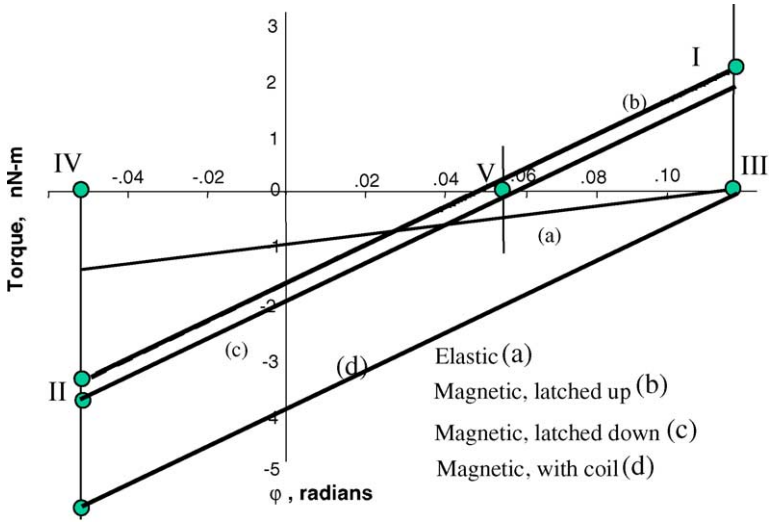

Fig. 5. Stability schematic for a type-2 magnetic actuator in a 25 mT external magnetic field. The initial upward angular deflection is approximately 0.12 rad.

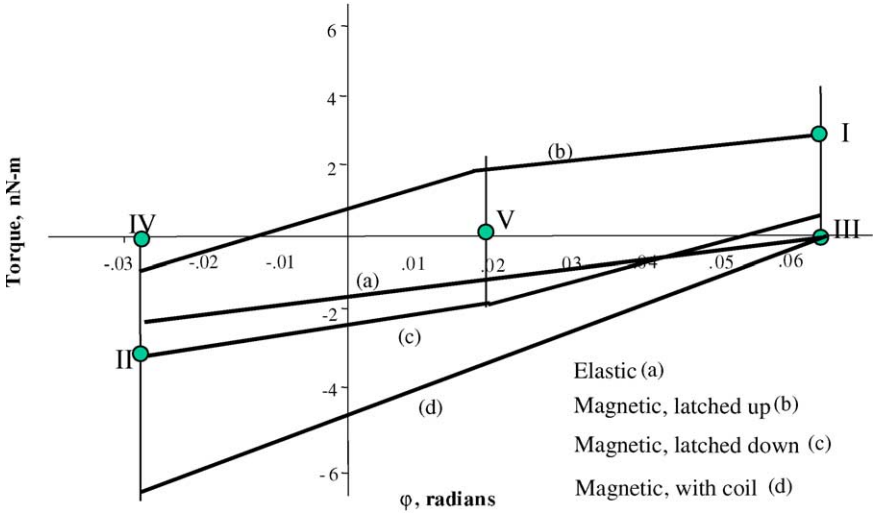

Fig. 6. Stability schematic for a type-3 magnetic actuator in a 10 mT external magnetic field. The initial upward angular deflection is approximately 0.06 rad.

ence of the lower (point IV) and upper (point III) mechanical stops (substrates). The angle corresponding to $\gamma = 0$ is shown (point V). This angle is different than $\varphi = 0$, due to the effect of the application angle of the magnetic field, α. This is done to regain symmetry of the latched states that is lost due to initial inclination angle of the beam (nonzero y-intercept). Device 3 displays a different relationship between the elastic torque and magnetic torque lines in Fig. 6 when compared to the graphical analysis in Figs. 4 and 5. The difference is that the upper magnetic torque line corresponding to the latched up state is readily stable at the lower stable position. That is, if the magnetization direction of the device could be instantly switched with a short current pulse through the coil, the pulse could be terminated and the magnetic torque line of the device would be switched from the bottom curve (c) to the upper curve (d). Then, without continued power to the integrated coil, the device would begin travel to the upstate. This behavior defines the short-pulse switching (SPS) regime.

Shape anisotropy is significant in providing for SPS. Device 2, with the lowest degree of shape anisotropy, has the lowest relative separation of the two magnetic torque branches (explained by Eq. (13)), and shows that the previous direction of magnetization is not significantly influential in determining a stable equilibrium. Furthermore, the relatively low degree of shape anisotropy in design 2 requires a significant magnetic field to saturate the magnetic material in the reverse direction. This combination of small magnetic torque curve separation and low anisotropy prevents the existence of the short-pulse switching regime for design 2. However, devices 1 and 3, with much higher shape anisotropy, have much greater separation of magnetic torque branches; however, the relative placement of the magnetic and elastic torque lines at the substrate positions still depends on the background magnetic field level and hinge stiffness. Fig. 4 demonstrates that design 1 does not satisfy the conditions for short-pulse switching, but could with a reduction in the background magnetic field and/or with an increase in the spring constant of the hinge. The vertical offset at $\gamma = 0$ is proportional to B (Eq. (12)), but the slope of the magnetic torque curve is proportional to B^2 (Eq. (7)). Therefore reduction in the external magnetic field would keep the upper magnetic torque line in excess of the elastic torque over a wider angular range, eventually reaching the bottom stable position. The dependence of the slope and offset of the magnetic torque curves on the magnetic field can be used to show the angular range over which the required relationship exists between the elastic and magnetic torques scales as B^{-1} for low stiffness hinges. It is for this reason that, regardless of shape anisotropy, short-pulse switching will not be observed for large actuation distances with background magnetic fields significantly larger than the 10 mT fields considered here. Continued reduction in the background magnetic field, however, reduces the available contact force holding the device in the latched state. Only design 3 exhibits the short-pulse switching regime in at least one direction.

In designs 2 and 3, the largest values of contact force are found at the limits of φ, i.e., at the top and bottom contact surfaces. Increased contact force is achieved with the greater movement of the beam tip. This is a result of incomplete magnetization, as the magnetic element is still realizing a greater magnetization at larger values of γ due to the greater external field component along the permalloy. Device 1, however, has the greatest shape anisotropy, and therefore the smallest valued denominator in Eqs. (13) and (7). Accordingly, device 1 is the only design where complete magnetization is predicted to occur at angles φ within the values corresponding to the two substrates. Therefore, the contact force realized at the latched states does not correspond to the greatest excess of the magnetic torque over the elastic torque.

4. Discussion

The purpose of this work was to explore the performance limits of the design space of a magnetic MEMS actuator and, in particular, to determine the region corresponding to the lowest switching energy necessary to move the device from one stable state to another. Since static models demonstrating the magnetic behavior of each of the designs have been generated, additional information related to the operation of the device may be determined.

4.1. Minimum latching field

The strength of the latching magnetic field can be reduced in each of these designs to find the minimum external field that satisfies the latching criterion (Eq. (14)) in each of the stable states. At equality of this minimum condition, the magnetic torque equals the elastic torque. The minimum switching field values can be obtained for each of the designs by reducing the external field until no solutions for latching exist at the substrates.

4.2. Minimum switching field/current

The minimum current supplied to the coil that produces a switching event can be determined by including the field produced by the coil in Eq. (7), giving

$$\Gamma_{\text{magnetic}} = VB\left(\operatorname{sgn}\gamma \min\left\{\frac{B_{\text{coil},x} + B\sin|\gamma| \pm H_c}{\sqrt{N_l{}^2 + \theta^2}}, M_{\text{sat}}\right\}\right) \times \cos\gamma \tag{19}$$

where the $\pm$ refers to the most recent magnetization state of the Ni/Fe. Furthermore, the component of the field in-plane with the beam acts to produce a magnetization opposite to the previous state. Equating Eq. (19) with the elastic torque yields the criterion for device switching presented in Section 1 (Eq. (1)). That is, if this coil field is great enough to overcome the coercivity and the in-plane component of the external field, less the elastic torque, the device will begin

Table 2
Minimum external coil current for onset of switching and contact force for different configurations

	Design 1	Design 2	Design 3
Minimum operating conditions			
$B_{external}$ (mT)	1.3	20	4.0
Latched conditions			
$B_{external}$ (mT)	10	25	10
M (T)	0.30	0.15	0.30
Min. B_{coil} (mT) for switching	0.7	1.5	0.7
I for min B_{coil} (mA)	40	120	40
B_{coil} (mT) for min. energy	0.8	1.9	0.8
Contact force (μN)	7.0	4.0	2.5
Contact force (μN) at $M = M_{fat}$	26	35	12

movement to the other latched region, producing a switching event. This is seen graphically by requiring the magnetic torque line to be depressed below the elastic torque line by application of B_{coil}. Using 0.3 mT as the value of the coercivity, the minimum coil field necessary to create a switching event is found to be 0.7 mT for designs 1 and 3 operating at 10 mT and 1.5 mT for design 2 operating at 25 mT. These minimum switching field values are summarized in Table 2 and form the lower bound asymptotes in Figs. 7 and 8, which describe the influence of the coil field on switching speed and switching energy, respectively. The minimum coil field values increase with the background magnetic field, and for devices with low anisotropy (design 2) the elastic torque may not be negligible. For example, switching from down to up for device 2 requires consideration of the elastic torque as shown in Fig. 5. Furthermore, these calculated minimum magnetic field values are translated into minimum currents supplied to the coil via Fig. 3.

For SPS, a larger current is needed since the applied magnetic field is now required to switch the magnetization of the magnetic material instead of just reducing it for the long-pulse method. The amount of extra current depends on the demagnetization factors, the elastic torque at the latched positions, the anisotropy torque, and the minor hysteresis loops of the ferromagnet, as will be shown in Part II.

4.3. Switching dynamics

Once the magnetic torque is no longer dominant, additional information can be obtained from these models by considering the dynamic behavior of the device during a switch-

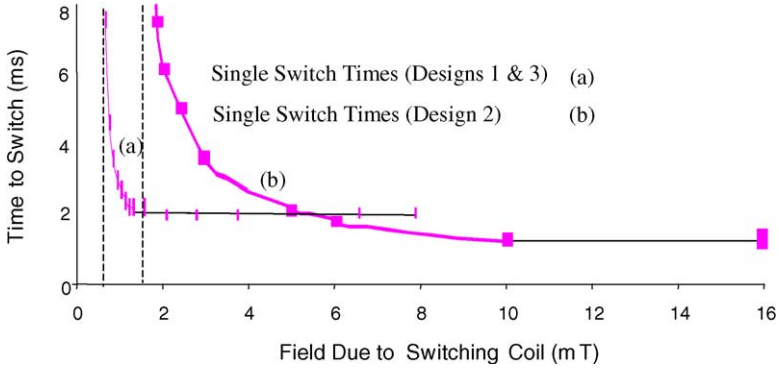

Fig. 7. Modeled minimum pulse width required to switch the devices.

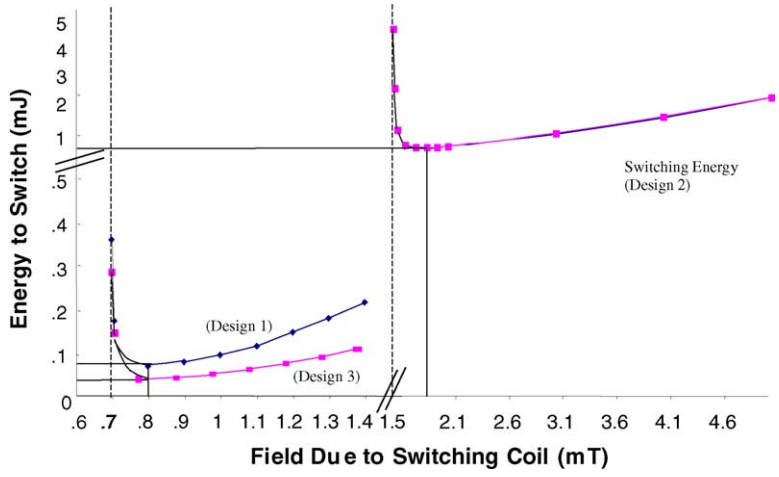

Fig. 8. Modeled energy to switch the devices.

ing event.

$$J\frac{d^2\phi}{dt^2} + C\frac{d\phi}{dt} + k_\phi(\phi - \phi^0) = \Gamma_{\text{magnetic}}, \quad \text{where :}$$

$$J = \frac{1}{2}m(x + X)^2, \quad k_\phi = \frac{Ewt^3}{6x} \tag{20}$$

where C is the damping parameter, x the hinge length, X the length of the permalloy portion of the beam, w the hinge width, t the hinge thickness, E the elastic modulus of the hinge material, and Γ_{magnetic} is given by Eq. (18). Damping parameter values similar to that measured by Judy and Muller [6] have a negligible impact on the calculated switching speeds at the reduced angular velocities characteristic of the designs and external magnetic fields of interest here; hence, damping is neglected in calculations of switching speed. From this analysis, estimates of the minimum switching energy and time were obtained.

Fig. 5 shows a model of device 2 with an initial inclination angle of 0.12 rad in a background external magnetic field of 25 mT. An additional component of the magnetic field is added by supplying a current to the integrated coil. The field generated by this coil acts to reduce the magnitude of the magnetic torque created by the presence of the permanent magnetic field thereby reducing the magnetization of the beam. The magnetic field generated by the coil must be great enough to bring the magnetic torque below the elastic torque line. This critical shift is shown in Fig. 5 as the curve (d). At this point, the net torque on the beam acts to reduce the inclination angle of the beam, φ, and the beam begins to accelerate toward the bottom substrate. For beams with low anisotropy, such as the beams described by Ruan et al. [1], the current pulse provided to the coil must remain powered until the unperturbed magnetic torque line is below the elastic torque line. Otherwise, once the coil is turned off, the beam will once again accelerate toward the upper substrate and switching will not occur. An instantaneous high current pulse is not sufficient since the lower magnetic torque line is below the elastic torque line while the beam is at the upper substrate. The beam must move the prescribed angular distance before the coil current is removed. In general, soon after this point, the coil current can be stopped, and the beam will continue to travel towards the bottom substrate, since the magnetic torque now acts in the opposite direction. As the device continues to move down, the magnetic element will magnetize further in the new direction, and the device latches against the bottom substrate.

According to Fig. 6, the analysis just described does not apply to device 3, in which the upper magnetic torque exceeds the elastic torque over the entire angular range of motion of interest. Therefore, in this case the coil must remain powered only until the magnetization in the device is sufficiently reversed so that when the coil field is removed, the magnetic torque will follow the bottom line. No portion of the upper magnetic torque line yields the bottom-latched position. Thus, for this device there is the added requirement that the magnetic torque must switch from the upper line to the lower line before the coil is turned off. However, the fact that the upper magnetic torque exceeds the elastic torque for all relevant φ introduces an asymmetry in the analysis for switching down and switching up. Since the upper magnetic torque line is stable at the lower substrate, simply moving from the lower line to the upper line is sufficient to produce switching of the device. Therefore, a short current pulse could be provided that will produce switching from the lower latched state to the upper latched state; and since no minimum amount of movement is required during the pulse to ensure stability, it is believed that this switching pulse may be made extremely short.

4.4. Contact force

The contact force in the latched states for each device was determined through Eq. (18) (Table 2). When the switching field is present, the magnetic torque is impacted, shown by reducing the upper magnetic torque line when switching from up to down (or increasing the lower magnetic torque line when switching from down to up). Once switching has been completed and the coil remains powered, it is apparent from Eq. (18) that the presence of the switching field produces a greater magnetization, and thus a greater magnetic torque. The degree of excess torque over the minimum provided by the coil influences the speed of switching (greater driving force), and produces a greater contact force in the latched states if the coil remains powered. This effect ceases to be enhanced once saturation of the magnetic material is realized during switching. The modeled contact forces (without coil current) for each device are shown in Table 2. The degree of magnetization is greater when the coil current is supplied. The decrease in the degree of magnetization when the coil current is terminated produces a commensurate reduction in the contact force. As anticipated, design 1 is predicted to have the greatest calculated contact force, over 7 μN. Both designs 1 and 3 retain 30% magnetization once the current to the coil is terminated, but design 3 experiences a contact force of 2.5 μN. The large decrease in the contact force between designs 1 and 3 is due mainly to the reduction in total permalloy volume as the degree of magnetization is calculated to be equal. This points to the increased width of design 1 as an advantage, allowing for more patterned Ni/Fe strips to be present on a given device. Design 2 has a greater contact force (4 μN) than design 3, even though it has the lowest shape anisotropy permalloy. The permalloy in design 2 does not exceed 15% magnetization in either latched state; however, the fact that the device is shorter than design 3 and is in a larger external field results in an increased contact force. Design 2 could be modified to have a much larger contact force if further increases in shape anisotropy were to be incorporated into the design. A contact force in excess of 30 μN could be obtained if the permalloy were shaped in such a way as to achieve saturation at 25 mT; however, this increased contact force requires higher energy to switch the device in the greater

background field of 25 mT. Furthermore, contact forces decrease with smaller switch sizes, as was shown in Section 2. Therefore, a larger benefit in contact force could be realized by raising the background magnetic field level from 10 to 25 mT in designs 1 or 3, but at the cost of increased energy to operate.

4.5. Minimum latching field

Table 2 shows that as the shape anisotropy is increased (going from design 2 to designs 1 and 3), the minimum external field necessary to achieve latched states decreases. This results from the increased magnetization due to the permalloy patterning. A greater external latching field, in turn, requires a greater switching magnetic field from the patterned coils, achieved by supplying increased current. This results in larger energy for a switching event.

4.6. Switching speed and energy

Fig. 7 shows the impact of the switching field on the switching time. Increased switching fields, from the on-chip coil, act to increase the degree of magnetization of the ferromagnetic element, resulting in an increased driving torque and lower switch time. This effect continues to the point where the switching field results in complete magnetization of the beam. Further increase in coil current does not reduce the switching time. This information is recast in Fig. 8, where the energy to switch the three different devices is shown as a function of the switching field. Below some threshold value, the switching field does not totally eliminate the contact force and results in beam movement. Above this threshold value, small increases in the switching field result in large reductions in switching speed and energy; however, this effect quickly diminishes, and soon the switching energy again begins to rise, as shown in Fig. 8. This means that the switching time does not decrease more than the square of the applied current to the coil that produces the switching field. The average energy to switch the device from one state to the other is plotted. These data are summarized in Table 3. Devices 1 and 3 are seen to require an order of magnitude less energy, and significantly less current due to their increased anisotropy and resultant ability to operate in lower magnetic fields. Furthermore, device 3 is predicted to require 40% less energy than device 1, owing to the SPS available from the downstate to the upstate. It should be noted that the long-pulse switching energy reported in Fig. 8 is calculated assuming a current pulse is supplied for the minimum duration that will produce a switching event. In most cases, the length of the current pulse was modeled to be approximately one-half the time for the beam to travel from φ_{top} to φ_{bottom}. However, the smaller device, design 2, has the potential for the shortest switching times, owing to its decreased mass and length. The lowest switching energy is expected to occur for design 3, in which one direction of switching is predicted to occur with very short current pulses and drastically reduced energy. An optimum design would have bi-directional SPS, patterned permalloy of designs 1 and 3, and the smaller beam size of design 2 to generate shorter beam travel times and larger contact forces sufficient for low resistance contact. For SPS, a larger current is required, but the contact forces and minimum external magnetic field for latching are unaffected.

5. Summary

A bistable magnetic actuation mechanism has been modified and adapted for determining the design space for micro actuators with large actuation distance and low switching energy. This has led to a modeled regime where switching pulses may be exceedingly short with concomitant extremely low switching energy. The comprehensive modeling considers initial deflections of the cantilever and application angle of the external magnetic field to regain stability symmetry. Additionally, the very significant effects of the coercivity and shape anisotropy of the ferromagnetic material determine the separation of the two branches of the magnetic torque and permit modeling of switching speed, contact force, and minimum operating conditions. Designs differing in size, ferromagnetic volume, and shape anisotropy were chosen and highlight the difference between the long-pulse and short-pulse switching (SPS) regimes. The designs vary in calculated values of contact force, with one design in excess of 7 μN at 10 mT, and larger contact forces possible with higher fields. They have switching speeds less than 3 ms, and suggest that switching energies could occur with as little as 84 μJ for the long-pulse regime and sub-μJ for SPS. SPS enables greater isolation to be achieved at greatly reduced switching energy, and minimal switching energy is achieved at the cost of reduced contact force. Compared to the previous data

Table 3
Modeled minimum switching times and energies for each design

Design 1	Design 2	Design 3
Minimum energy		
85 μJ to switch, 10 mT external field, 1.2 ms pulse, 0.8 mT–48 mA through coil	1.0 mJ to switch, 25 mT external field, 2.1 ms pulse, 2.4 mT–126 mA through coil	(98 + ∼0)/2 = ∼50 μJ to switch (average), 10 mT external field, 1.4 ms pulse, 0.8 mT (from coil) to 48 mA
Minimum switch time[a]		
1.1 ms to switch @ 1.9 mT (116 mA)	0.6 ms to switch @ 12 mT (700 mA)	1.3 ms to switch @ 1.9 mT (116 mA)

[a] Higher current does not reduce switching time.

reported based on the long-pulse switching mechanism [1], the modeled relays in this study would actuate over much larger distances, 100 μm versus 12 μm, with correspondingly slower switching speeds, 3 ms versus 0.4 ms, and with similar energies, 84 μJ for long-pulse versus 93 μJ, than previously reported [1].

Acknowledgments

Significant contributions by Eric M. Prophet, Balam A. Willemsen, and Jürgen Musolf of Superconductor Technologies Inc. in the form of technical insight and valuable discussion are greatly appreciated. This material is based upon work supported by the Defense Advanced Research Projects Agency, Defense Science Office, DARPA Order No. J607 Total Agile RF Sensor Systems (TASS) issued by DARPA/CMD under Contract #MDA972-00-C-0010.

References

[1] M. Ruan, J. Shen, C.B. Wheeler, Latching electromagnetic relays, J. Microelectromech. Syst. 10 (2001) 511–517.
[2] J.J. Yao, RF MEMS from a device perspective, J. Micromech. Microeng. 10 (2000) R9–R38.
[3] A.K. Chinthakindi, D. Bhusari, B.P. Dusch, J. Musolf, B.A. Willemsen, E. Prophet, M. Roberson, P.A. Kohl, Electrostatic actuators with intrinsic stress gradient. Part-I. Materials and structures, J. Electrochem. Soc. 149 (2002) H139–H145.
[4] A.K. Chinthakindi, P.A. Kohl, Electrostatic actuators with intrinsic stress gradient. Part-II, J. Electrochem. Soc. 149 (2002) H146–H152.
[5] G.D. Gray, M.J. Morgan, P.A. Kohl, Electrostatic actuators with expanded tuning range due to biaxial intrinsic stress gradients, J. Microelectromech. Syst. 13 (2004).
[6] J. Judy, R. Muller, Magnetically actuated, addressable microstructures, J. Microelectromech. Syst. 6 (1997) 249–256.
[7] C. Ahn, M. Allen, A fully integrated surface micromachined magnetic microactuator with a multilever meander magnetic core, J. Microelectromech. Syst. 2 (1993) 15–22.
[8] W. Taylor, M. Allen, Fully integrated magnetically actuated micromachined relays, J. Microelectromech. Syst. 7 (1998) 181–191.
[9] J. Wright, Y. Tai, S. Chang, A large-force fully-integrated MEMS magnetic actuator, in: Technical digest: 1997 International Conference on Solid-State Sensors and Actuators: Transducers'97, vol. 2, 1997, pp. 793–796.
[10] M. Campanu, J. Boyd, P. Hesketh, Design, fabrication, and testing of a bistable electromagnetically actuated microvalve, J. Microelectromech. Syst. 9 (2000) 181–189.
[11] C. Liu, Micromachined magnetic actuators using electroplated permalloy, IEEE Trans. Magn. 35 (1999) 1976–1985.
[12] J. Jackson, Classical Electrodynamics, 3rd ed., Wiley, New York, 1999.
[13] E. Fullin, J. Gobet, et al., A new basic technology for magnetic micro-actuators, in: MEMS 1998 Workshop, Heidelberg, January 25–29, 1998.
[14] H. Hosaka, Micro Electro Mechanical Systems Conference, IEEE, Fort Lauderdale, Florida, February 7–10, 1993.

Biographies

Gary D. Gray, Jr. received the B.S. degree in chemical engineering from the Georgia Institute of Technology, Atlanta, in 2000. He is currently working toward the M.S. degree in physics and the Ph.D. degree in chemical engineering at the same.

Paul A. Kohl received a B.S. degree in chemistry from Bethany College in 1974 and Ph.D. from The University of Texas at Austin in 1978. He was employed by AT&T Bell Laboratories from 1978 to 1989 and joined the Georgia Institute of Technology by 1989, where he is now a Regents' Professor.